TEMPERATURE DISTRIBUTION MODELING OF A WELDED JOINT BY THE USE OF THERMOGRAPHIC IMAGES

Eduardo José Fernandes Rocha [1]
Tiago de Sousa Antonino [2]
[1]Universidade Federal de Pernambuco – Departamento de Engenharia Mecânica, Av. da Arquitetura, Cidade Universitária, Zip Code: 50740-550. Recife–PE, Brazil. Fax: +55(81)21268232.
[2]Instituto Federal de Educação, Ciência e Tecnologia de Pernambuco – IFPE, Av. Professor Luiz Freire, 500, Cidade Universitária, CEP 50740-540, Recife–PE, Brazil.
edujfr@gmail.com, tiago_antonino@yahoo.com.br.

Ricardo Artur Sanguinetti Ferreira[1]
Pablo Batista Guimarães[2]
Paternak de Souza Barros[1]
José Manoel de Sousa[1]
Yogendra Prasad Yadava[1]
José Maria Andrade Barbosa[1]
Roberto de Araújo Alécio[3]
[1]Universidade Federal de Pernambuco – Departamento de Engenharia Mecânica, Av. da Arquitetura, Cidade Universitária, Zip Code: 50740-550. Recife–PE, Brazil. Fax: +55(81)21268232.
[2]Instituto Federal de Educação, Ciência e Tecnologia de Pernambuco – IFPE, Av. Professor Luiz Freire, 500, Cidade Universitária, CEP 50740-540, Recife–PE, Brazil.
[3]Instituto Federal de Educação, Ciência e Tecnologia de Alagoas – IFAL, Rua Barão de Atalaia, S/N, Centro, CEP 57020-510, Maceió-AL, Brazil.
ras@ufpe.br, pabloguimaraes@recife.ifpe.edu.br, nark1945@yahoo.com.br, jmanoelsousa@gmail.com, yadava@ufpe.br, jmab@ufpe.br, ralecio@gmail.com.

Abstract*. The aim of this work is to perform temperature distribution studies in an electric arc filling welding process by the application of a mathematical model which was validated with the aid of a heat measuring device operating in the infrared spectrum range. The numerical methodology was based on the commercial finite element analysis software Abaqus for performing three-dimensional analysis of the heat involved in the filling process. The heat source motion was modeled based on Goldak's double ellipsoid and the subsequent volumetric energy distribution, which include the physicothermal properties of the material and the respective boundary conditions inherent in the system. The experimental field performed through the automated GMAW welding process in the flat 2G position, which consisted of a rectangular API 5L X80 steel panels of dimensions 150 x 80 x 7.5 mm and a 4 mm chamfer, provided the basis for feeding the computer data.*

Keywords: *Numerical modeling, infrared thermography, temperature field, welding, API 5L X80 steel.*

1. INTRODUCTION

The occurrence of the so called thermal stresses, generated by the strong thermal gradient employed in welding which as a result promotes geometric distortions and the generation of non-uniformly distributed internal stresses (residual stresses), is observed in these welded parts. These stresses most of the time are undesirable due to the possibility of damaging the quality of the welded components (Masubuchi, 1980; Parlane *et al*., 1981). The determination of residual stresses in welded pipelines may be accomplished by experimental procedures such as the techniques based on blind bore, X-ray diffraction, neutron diffraction, and ultrasound (Yaghi *et al*., 2010 and 2011). If the set of properties is available during the numerical simulation and the generated mesh is sufficiently refined, then the temperature fields and residual stresses due to welding can be accurately obtained along the model, thus making the finite element method highly effective (Yaghi *et al*., 2011) and with large margins for obtaining results very similar with those obtained from the infrared system (IR), since it provides direct evidences of transient temperatures and the real boundary conditions of the system under study (Camilleri *et al*., 2009). In view of this technique, it is possible to see the light artificially within the infrared spectrum which makes it an extension of the human vision (Michalski *et al*., 2013). In the proposed work, the phase changes in the solid state (γ↔α), which influence the temperature field and the generation of residual stresses due to the modification of the specific volume through the variation of the thermophysical properties that change with temperature, was considered indirectly (Bhadeshia, 2004; Francis and Bhadeshia, 2007)

2. EXPERIMENTAL METHOD

The base metal used in this study is the API 5L X80 steel pipe with a thickness of 19 mm, a nominal diameter of 864 mm (34") and a chemical composition depicted in Tab.1.

Table 1. Chemical composition of the API 5L X80 steel pipe (% mass).

C	S	N	Al	Si	P	Ti	V
0.03	0.003	0.0054	0.027	0.21	0.013	0.017	0.023
Cr	**Mn**	**Ni**	**Cu**	**Nb**	**Mo**	**B**	**Ca**
0.158	1.78	0.013	0.008	0.071	0.183	0.0001	0.0032

The filler metal used was the GMAW solid wire, diameter 1.2 mm, ER70S-6 model, according to the AWS / ASME SFA - 5:18 standard (AWS, 2001 and ASME, 2001).The deposition of the weld bead occurred at a butt joint with a Biesel angle of 45° along the longitudinal direction of the specimen with dimensions of 150 mm x 80 mm x 7.5 mm. The applied automated GMAW process (Fig. 1) is based on the parameters contained in Tab. 2.

Table 2. Welding parameters used in the experiment.

Current [A]	192
Voltage [V]	18.4
Weld speed [m/s]	0.00278
Contact tip-to-work distance (CTWD) [m]	0.0016
Wire feed speed [m/s]	0.167
Shielding gas flow rate (75% Ar+25% CO_2)[lts/min]	16
Polarity	CC+
Thermal efficiency of the process	85%
Welding average time [sec]	36
Weld bead length [mm]	100
Weld position	Horizontal 2G

Figure 1. Automated GMAW process utilized in this work.

3. GMAW FINITE ELEMENT MODELING

The welding GMAW is considered to only cause melting of the metal without vaporization. Variations of the thermophysical properties of the material are considered with temperature, which leads to a non-linear analysis. A transient analysis was conducted in order to obtain the temperature field as a function of time for the thermal analysis of this study, apart from heat transfer by conduction which takes losses by convection and radiation into account.

3.1 Thermal analysis

In most of the fusion welding processes, a source of concentrated heat and high intensity is applied and moved along a joint position (Marques *et al*., 2011). Heat conduction through a solid, considering the time t and related to a tri-orthogonal cartesian coordinates (x, y, z) can be expressed by Eq. (1) (Wainer *et al*., 1992):

$$\frac{\partial}{\partial x}\left(K_T\frac{\partial T}{\partial x}\right)+\frac{\partial}{\partial y}\left(K_T\frac{\partial T}{\partial y}\right)+\frac{\partial}{\partial z}\left(K_T\frac{\partial T}{\partial z}\right)+q_0=\rho c_P\frac{\partial T}{\partial t} \quad (1)$$

In this equation T represents temperature, q_0 heat source, x, y, z the tri-orthogonal cartesian coordinates, t for time, K_T thermal conductivity, ρ the density e CP the specific heat of the material. During the welding operation, the material exchanges heat with the surrounding environment by convection and radiation. Heat losses by convection is represented by the equation $\Phi_c = h_c(T - T_\infty)$, while heat losses by radiation is expresses by $\Phi_r = \sigma\varepsilon(T^4 - T_\infty^4)$, where hc is the coefficient of convection, T the surface temperature of the object, T∞ the temperature of the surrounding fluid (T∞ = 27ºC), σ Stefan – Boltzmann constant (σ = 5,7 x 10-8 $Wm^{-2}K^{-4}$) and ε the emissivity of the object (ε = 0,91) (Rocha, 2012). Table 3 shows the results of thermophysical properties of API 5L X80 (Antonino *et al*., 2014).

Table 3. Experimentally measured results of the thermophysical properties of API 5L X80.

Temp. [ºC]	Thermal Conductivity [W/m ºC]	Coeff. of Thermal Diffusivity [m^2/seg]	Coeff. of Thermal Expansion [$ºC^{-1}$]	Specific Heat [J/kg ºC]
0	51.062	1.400E-05	8.50E-06	571.235
100	51.062	1.315E-05	8.50E-06	571.235
200	47.324	1.198E-05	8.50E-06	571.235
300	43.840	1.087E-05	8.50E-06	571.235
400	40.424	9.670E-06	8.50E-06	614.841
500	29.634	8.237E-06	8.50E-06	668.617
550	33.546	7.358E-06	7.50E-06	730.831
600	26.461	5.991E-06	7.50E-06	780.774
650	18.019	3.647E-06	7.50E-06	868.623
700	14.874	2.865E-06	7.50E-06	977.091
750	11.386	2.149E-06	-5.00E-06	841.431
800	14.735	2.735E-06	-2.50E-06	790.265
900	14.735	2.149E-06	5.00E-06	608.333
1200	14.735	2.149E-06	8.50E-06	681.529

3.2 Moving heat source

The subroutine destined to move the heat source generated by the GMAW torch is called DFLUX which sequentially applies the heat flow to the nodes as a function of time, according to the adopted welding speed (Brickstad and Josefson, 1998; Karlsson, 2007; Jiang *et al*., 2011).

The adopted model of heat source was the Goldak double-ellipsoid (Fig. 2) that combines two different ellipsoids, one at the frontal quadrant (Eq. 2) and the other at the rear quadrant (Eq. 3) (Goldak and Chakravarti, 1984; Goldak and Akhlaghi, 2005). This will represent the energy flow volumetric distribution by simulating heat input to the weld joint.

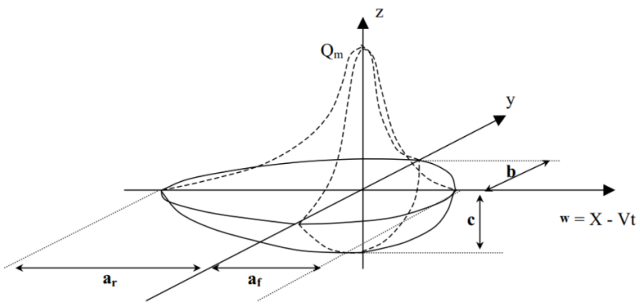

Figure 2. The Double-Ellipsoid Model or the Goldak (Goldak and Chakravarti, 1984).

$$P_f(x,y,z) = f_f \eta U I \frac{6\sqrt{3}}{a_f b c \pi^{3/2}} e^{\left(\frac{-3x^2}{a_f^2}\right)} e^{\left(\frac{-3y^2}{b^2}\right)} e^{\left(\frac{-3z^2}{c^2}\right)} \quad (2)$$

$$P_r(x, y, z) = f_r \eta U I \frac{6\sqrt{3}}{a_r b c \pi^{3/2}} e^{\left(\frac{-3x^2}{a_r^2}\right)} e^{\left(\frac{-3y^2}{b^2}\right)} e^{\left(\frac{-3z^2}{c^2}\right)} \quad (3)$$

The energy distribution between the front and the rear of the heat source is represented by the variable $f_f=2a_f/a_f+a_r$ and $f_r=2a_r \; a_f+a_r$, where $f_f + f_r = 2$.The parameters U, I and η depend on the welding process and the parameters b and c can be measured by weld pool macrography of the welded joints. The parameters a_f, a_r, f_f and f_r are calculated based on the parameters b and c, where $a_f = 0{,}5\,c$ and ar = 2c.

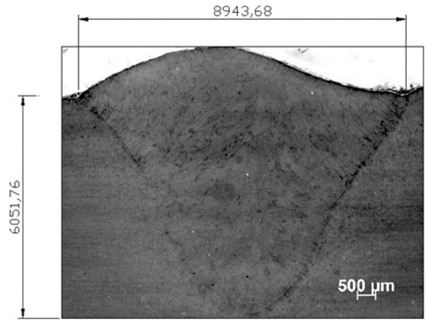

Figure 3. Macrography of the API 5L X80 steel welded joints, after a nital acid attack at 5% and an increase of 13 X.

Table 4 shows the geometric parameters of the Goldak heat source used in this work.

Table 4. Values of the heat source parameters.

Parameter	Value
B	0.004472 [m]
C	0.00605 [m]
a_f	0.003025 [m]
a_r	0.0121 [m]
f_f	0.4
f_r	1.6

3.3 Finite element mesh generation and boundary conditions

The three-dimensional element meshing in the finite element model used: DC3D8 (Fig. 4). It consists of 75,570 elements and 85,822 nodes and was estimated after the convergence tests. Then it was refined in the melted zone (MZ) and also in the heat-affected zone (HAZ). A mechanical boundary condition is available in the ABAQUS/ENCASTRE software and mechanical fixing was created in the lower fixed edges, ensuring the absence of degrees of freedom in the model as shown in Fig. 5.

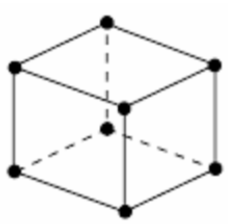

Figure 4. Finite element type DC3D8.

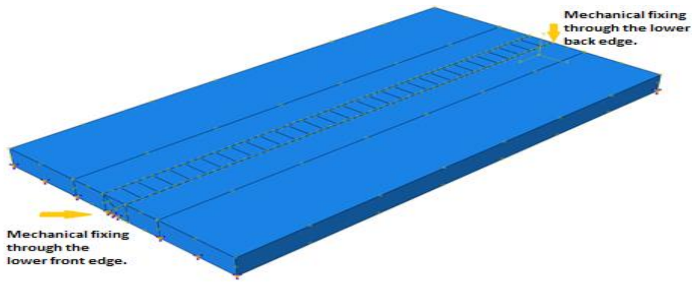

Figure 5. Boundary conditions for mechanical attachment.

4. MEASUREMENTS BY THERMOGRAPHY

In order to validate the temperature distribution model on the other side of the welding, the infrared thermography (IR) was chosen since it is a non-destructive testing technique that involves "contactless" measurement (Fig. 6), a fact relevant for this work due to the elevated temperatures present in welding and the need of using high precision instruments (Zeng *et al.*, 2009).

The emissivity is the most important feature of the surface of an object. The value used in this study corresponds to ε = 0.9134 ± 0.068 and was measured in a previous study (Rocha, 2012) where in a similar fashion, the surface of the specimens were sanded and painted matt black with spray paint, with the aim of reducing emissivity fluctuations. The value introduced into the two digit thermal camera was actually 0.91. Reference emissivity values at 0.9 and therefore very close to that used in this experiment were applied by other authors in temperature field studies with respect to the welding arc (Camilleri *et al*., 2009; Gery *et al*., 2005; Gannon L, *et al*., 2010).

Figure 6. Experimental bench for IR measurements.

5. RESULTS AND DISCUSSION

5.1 Temperature field image

The temperature fields and thermal cycles obtained experimentally and numerically on the rear face of the tested material show a high compatibility of temperature indications, Fig. 7.

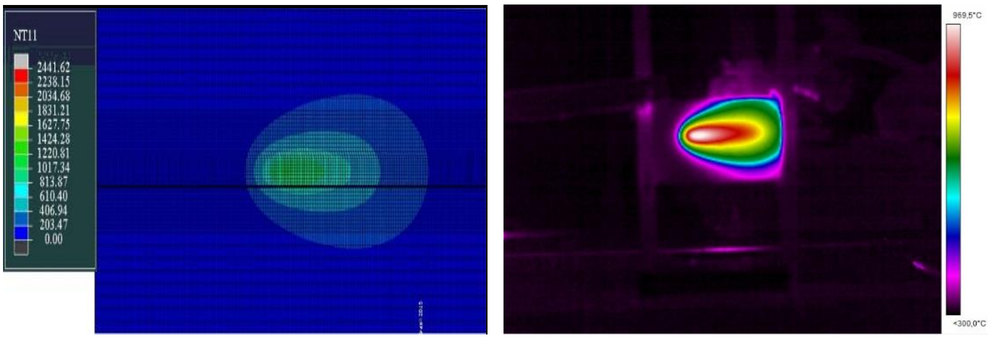

a) b)

Figure 7. Photography of temperature fields after a distance of 66mm covered by the welding torch, where a) FEM and b) IR. Both pictures represent the welding torch moving from the right to the left direction of the paper.

5.2 Numerically and experimentally obtained termal cycles

Figure 8 presents similar heating and cooling curves comparing the numerical and experimental results and figure 9 shows a specimen design which includes points to clarify the thermal cycles.

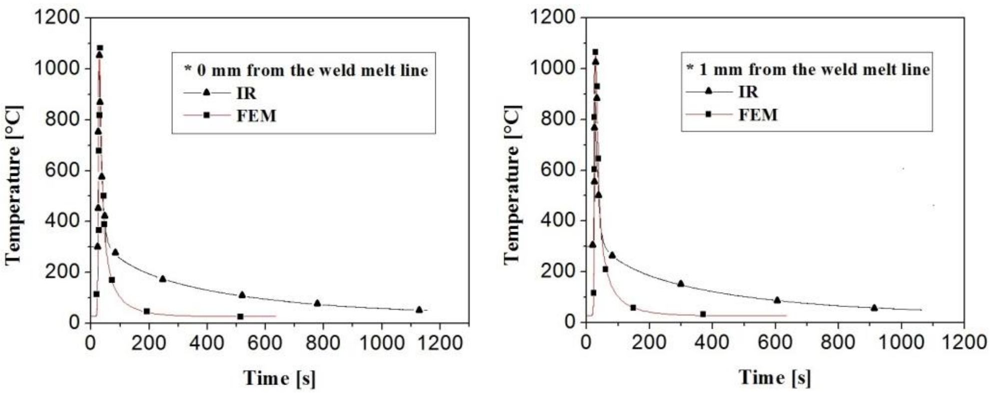

a) b)

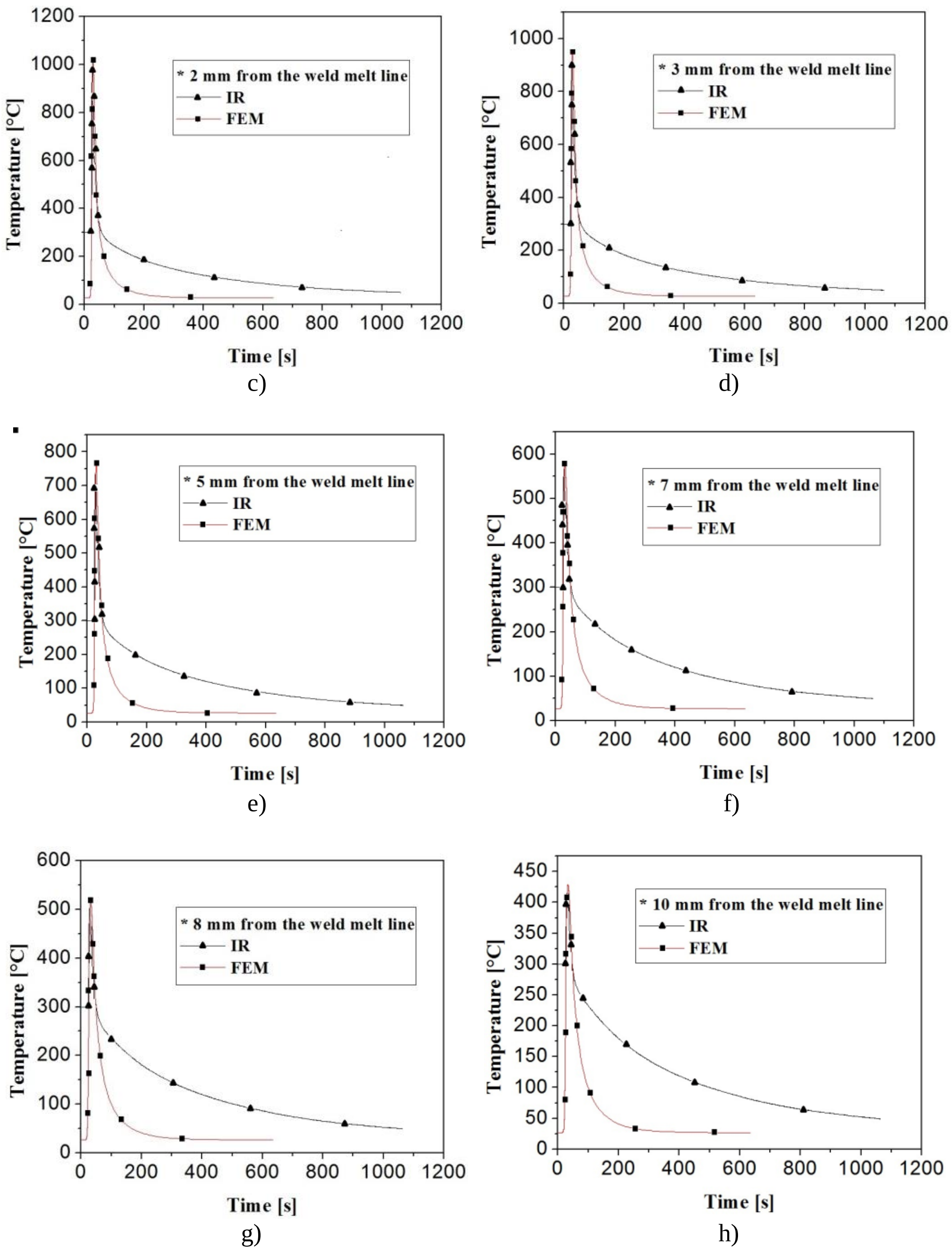

Figure 8. Numerically (FEM) and experimentally (IR) measured thermal cycles and their respective relative distances to the weld melt line (WML): a) 0 mm, b) 1 mm, c) 2 mm, d) 3 mm, e) 5 mm; f) 7 mm, g) 8 mm), h) 10 mm.

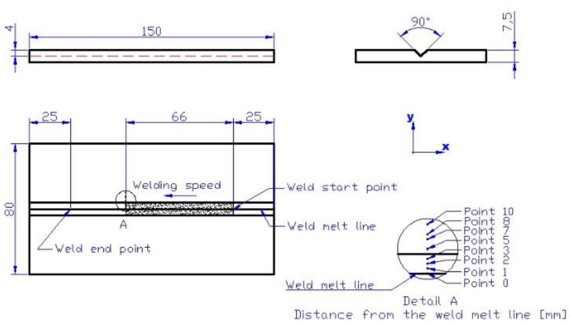

Figure 9. The zero point is found at center of the weld melt line (WML), 66 mm away from the initial point.

The disparity leads to negligence which was presented in the FEM mathematical model, since the mathematical approaches consider the mass of the welded material as infinite, this way resulting into a very rapid cooling process especially in regions with temperatures below 500°C. The entire region can be considered as unresponsive to the said validation considering that in these temperature ranges there is not any microstructural change in the base metal.

Table 5 shows a comparison of the summed peak temperatures reached on the opposite side of the welding conducted in this work, considering the experimental and numerical techniques with respect to the WML.

Table 5. Comparison between peak temperatures, according to the distance of the points with respect to the WML.

Points[mm]	FEM[°C]	IR[°C]	Error [%]
0	1083	1045	3,51
1	1067	1033	3,19
2	1021	983	3,72
3	951	903	5,05
5	769	692	10,01
7	578	486	15,92
8	521	404	22,46
10	428	389	9,11

Point temperatures of up to 980 °C, at distances of 0, 1 and 2 mm from the WML, showed very consistent readings with an error of about 3%.As these readings approach the temperature range of 800 and 500 ° C (the readings were between 950 and 520 °C based on FEM), the respective distant points 3, 5, 7 and 8 mm from the WML would present an error that will be subjected to expansion as it varies from 5 to 22%. This is due to the phenomenon of iron allotropy such that there will inevitably be a period of time necessary for the thermal equilibrium of the specimen through the phase changes that occur at these temperatures, resulting to a delay or thermal inertia detected only by the IR system and unnoticed by the FEM system. In this regard, the point is found at 10 mm from the WML when the temperature field is found to be moving away from the range mentioned in the previous item, indicating that the reading process is resumed with a greater integration between both systems and the error amplitude at around 9%.

6. CONCLUSIONS

1) When the experimental and numerical results are compared, it can be seen that the thermal cycles on all selected points in Fig.8, presented heating curves and similar peak temperatures.

2) This same analysis when applied to the cooling curve also showed a good agreement until a temperature of 300°C.

3) The peak temperature is well represented by the numerical model from 0,1,2,3,5 and 10 mm, which are points from the WML, when the maximum error is 10%. Points 7 to 8 mm to the WML were distant from the real ones obtained by the IR system, with errors of 15.92% and 22.46% respectively.

4) The temperature fields and thermal cycles obtained numerically and experimentally at the rear face of the material tested demonstrate a wide compatibility of temperature indications.

5) The results of the simulation show that the model is very sensitive and a proper disposition of the welding parameters can present in a very consistent way what actually occurs. This simulation model can be used as a convenient tool to investigate the effect of welding parameters in the GMAW process.

6) Infrared thermography along with numerical simulation form a solid basis for the study of temperature distribution during welding, which promotes the influences for distortion and residual stresses analysis in metallic structures.

7) The numerical simulation can complete the temperature distribution on the front face of the weld, which performed together due to the high temperatures (above 20,000 K) present in the welding arc.

7. REFERENCES

Masubuchi, K., 1980. *Analysis of Welded Structures. Residual Stress and Distortion and Their Consequences*. Pergamon Press, Oxford. New York.

Parlane, A.J.A., Allen, J.S., Harrison, J.D., Leggatt, R.H., Dwight, J.B., Bailey, N., Procter, E. and Saunders, G.G., 1981. *Residual Stresses and their Effect*. The Welding Institute, U.K.

Yaghi, A.H., Hyde, T.H., Becker, A.A., Sun, W., Hilson, G., Simandjuntak, S., Flewitt, P.E.J., Pavier, M.J. and Smith, D.J.A., 2010. Comparison between Measured and Modelled Residual Stresses in a Circumferentially Butt-Welded P91 Steel Pipe. *ASME Journal of Pressure Vessel Technology*, Vol. 132, p. 1-10.

Yaghi, A.H., Tanner, D.W.J., Hyde, T.H., Becker, A.A. and Sun, W., 2011. Abaqus Thermal Analysis of the Fusion Welding of a P92 Steel Pipe. *SIMULIA Customer Conference2011*. Nottingham, UK.

Camilleri, D., Gray, T. and Comlekci, T., 2009. *Use of Thermography to Calibrate Fusion Welding Procedures in Virtual Fabrication Applications*. Department of Mechanical Engineering, University of 01Strathclyde-UK.

Michalski, L.K., Eckersdorf, J. and Kucharski, J., 2013. *Temperature Measurement.* McGhee - Copyright © 2001 John Wiley & Sons Ltd, 2nd edition.

Bhadeshia, H.K.D.H., 2004. Developments in Martensitic and Bainitic Steels: Role of the Shape Deformation. *Materials Science and Engineering*, Vol. 378, p. 34–39.

Francis, J.A., Bhadeshia, H.K.D.H., Withers, P.J., 2007. Welding Residual Stresses in Ferritic Power Plant Steels. *Materials Science and Technology*, Vol. 23, p. 1009-1020.

AWS A5.18 - American Welding Society, 2001. *Specification for Carbon Steel Electrodes and Rods for Gas Shielded Arc Welding*.

ASME - The American Society of Mechanical Engineers, 2001. *Boiler and Pressure Vassel Code*. Section II – C, Vol. 49, SFA5.18 and SFA 5.20.

Marques, P.V., Modenesi, P.J. and Bracarense, A. Q., 2011. *Soldagem: Fundamentos e Tecnologia*. UFMG, Belo Horizonte, Brazil.

Wainer, E., Brandi, S.D. and Mello, F.D.H.,1992. *Soldagem: processos e metalurgia*. Edgard Blücher Ltda, São Paulo, Brazil.

Rocha, E.J.F., 2012. *Uso da Termografia na Análise do Resfriamento de Chapas Soldadas*. MSc. thesis. Department of Mechanical Engineering, Federal University of Pernambuco, Recife, Brazil.

Antonino, T.S., Guimarães P.B., Alécio, R.A., Yadava, Y.P. and Ferreira, R.A.S., 2014. Measurements of the Thermophysical Properties of the API 5L X80 Steel. *Materials Sciences and Applications*.

Brickstad, B. and Josefson, B.L.A., 1998. Parametric Study of Residual Stresses in Multi-pass Butt Welded Stainless Steel Pipes. *International Journal of Pressure Vessels and Piping*, Vol. 75, p. 11-25.

Karlsson, H., 2007. *Sorenson Inc. Abaqus User Subroutines Reference Manual*,Version 6.7. USA. “DFLUX” Section 1.1.3, “USDFLD” Section 1.1.40.

Jiang, W.C., Wang, B.Y., Gong, J.M. and Tu, S.T., 2011. Finite Element Analysis of the Effect of Welding Heat Input and Layer Number on Residual Stress in Repair Welds for a Stainless Steel Clad Plate. *Materials and Design*, p. 2851–2857.

Goldak, J. and Chakravarti, A., 1984. A New Finite Element Model for Welding Heat Sources. *Metallurgical Transactions*, Vol. 15, p. 299-305.

Goldak, J.A. and Akhlaghi, M., 2009. Computational Welding Mechanics. *Springer New York*, p. 30-35.

Zeng, Z., Wang, L., Wang, Y. and Zhang, H., 2009. Numerical and experimental investigation on temperature distribution of the discontinuous welding. *Computational Materials Science*, Vol. 44, p. 1153–1162.

Gery, D., Long, H. and Maropoulos, P., 2005. Effects of welding speed, energy input and heat source distribution on temperature variations in butt joint welding. *Journal of Materials Processing Technology*,Vol. 167, p. 393-401.

Gannon, L., Liu, Y. and Smith, M., 2010. Effect of welding sequence on residual stress and distortion in flat-bar stiffened plates. *Marine Structures*, Vol. 23, p. 385-404.

8. RESPONSIBILITY NOTICE

The authors are the only responsible for the printed material included in this paper.